An Observational Study on the Latitudes Where Wave Forcing Drives Brewer–Dobson Upwelling

TIEHAN ZHOU

NASA Goddard Institute for Space Studies, and Center for Climate Systems Research, Columbia University, New York, New York

MARVIN A. GELLER

School of Marine and Atmospheric Sciences, Stony Brook University, Stony Brook, New York

WUYIN LIN

Atmospheric Sciences Division, Brookhaven National Laboratory, Upton, New York

(Manuscript received 28 July 2011, in final form 16 December 2011)

ABSTRACT

The 40-yr ECMWF Re-Analysis (ERA-40) data are analyzed to demonstrate that wave forcing at lower latitudes plays a crucial role in driving the tropical upwelling portion of the Brewer–Dobson circulation. It is shown that subtropical wave forcing is correlated with tropical upwelling on both intraseasonal and interannual time scales when transient waves are taken into account, and that tropical wave forcing exerts its influence on tropical upwelling via its body force on the zonal mean flow.

1. Introduction

Since the pioneering works of Brewer (1949) and Dobson (1956), the stratospheric meridional circulation, known as the Brewer–Dobson circulation (BDC), has been recognized as an integral part of the global climate system (Murgatroyd and Singleton 1961; Dunkerton 1978; Rosenlof and Holton 1993; Holton et al. 1995; Haynes 2005). Model simulations show a strengthening of the BDC in response to greenhouse gas–induced climate change (Rind et al. 1990, 1998; Butchart et al. 2000; Butchart and Scaife 2001; Sigmond et al. 2004; Butchart et al. 2006, 2010, 2011; Fomichev et al. 2007; Li et al. 2008; Garcia and Randel 2008).

Adiabatic cooling in the upwelling branch of the BDC leads to the ''tropical cold point'' while adiabatic warming in the downwelling branch keeps temperatures above radiative equilibrium over the winter polar region (Andrews et al. 1987; Yulaeva et al. 1994; Salby and Callaghan 2002; Ueyama and Wallace 2010). Variations of the BDC have important implications for stratospheric ozone and its recovery (WMO/UNEP 2011, and references therein), water vapor concentrations and other chemical species (Ko et al. 1985; Holton 1990; Mote et al. 1996; Randel et al. 1999a, 2006; Zhou et al. 2001), and the age of stratospheric air (Hall and Plumb 1994; Waugh and Hall 2002; Austin and Li 2006; Austin et al. 2007; Oman et al. 2009; Waugh 2009; Garcia et al. 2011). The extratropical part of the BDC is relatively better understood than tropical upwelling (i.e., the tropical part of the BDC). Wave dissipation in the stratosphere drives the poleward transport and forces mean downwelling at high latitudes (McIntyre and Palmer 1983, 1984; Haynes and McIntyre 1987; McIntyre 1990, 1999; Haynes et al. 1991; Holton et al. 1995; Waugh 1996), which is capsulized as the ''downward control'' principle (Haynes et al. 1991)—that is, in the steady state, the extratropical residual mean vertical velocity on a given pressure level is controlled exclusively by the distribution of the wave drag above that level. The downward control principle (Haynes et al. 1991) is conventionally formulated as

Corresponding author address: Tiehan Zhou, NASA Goddard Institute for Space Studies, and Center for Climate Systems Research, Columbia University, New York, NY 10025.
E-mail: tz2131@columbia.edu

DOI: 10.1175/JAS-D-11-0197.1

$$\overline{w}^*(\varphi, z) = \frac{1}{\rho_0 \cos\varphi} \frac{\partial}{\partial \varphi} \left[\int_z^{\infty} \left(\frac{\rho_0 a D \cos^2\varphi}{\overline{m}_{\varphi}} \right)_{\overline{m}=\text{const}} dz' \right], \quad (1)$$

where $\overline{w}^*$ is the residual mean vertical velocity, φ the latitude, z the log pressure height, ρ_0 the reference density profile, a the radius of the earth, D the wave forcing, $\overline{m} = a\cos\varphi(\overline{u} + \Omega a \cos\varphi)$ the zonal mean angular momentum, $\overline{u}$ the zonal mean zonal wind, Ω the angular velocity of the earth, and dz' the vertical projection of a segment of the $\overline{m}$ curve; the subscript φ denotes partial derivative with respect to latitude, and the integration is along angular momentum contours.

Since conservation of mass requires that the total upwelling mass fluxes compensate the total downwelling mass fluxes on any pressure level, the principle of downward control has been exploited to derive mass fluxes from the troposphere to the stratosphere in the tropics and an area-averaged tropical upwelling velocity at 100 hPa by calculating downward mass fluxes across the 100-hPa level in the extratropics of both hemispheres (Holton 1990; Rosenlof and Holton 1993; Rosenlof 1995; Randel et al. 2002, 2008). Before the seminal work of Haynes et al. (1991), the residual velocities were calculated from thermodynamic balance (Murgatroyd and Singleton 1961; Solomon et al. 1986; Gille et al. 1987; Rosenfield et al. 1987; Shine 1989). Later on, upwelling velocities could also be estimated via aircraft (Boering et al. 1996) and satellite (Mote et al. 1996; Niwano et al. 2003) measurements of trace constituents.

However, consensus has not been reached on how wave forcing drives tropical upwelling in the lower stratosphere. Some studies (Yulaeva et al. 1994; Holton et al. 1995; Holton 2004) argued that tropical upwelling is remotely driven by high-latitude wave forcing, which was termed the ''extratropical suction pump'' (Holton et al. 1995). Meanwhile, Rosenlof (1995) pointed out that tropical stratospheric upwelling is directly related to the subtropical wave forcing at the ''turnaround latitudes'' (i.e., the latitudes where the residual mean vertical velocity switches from upward to downward). The importance of subtropical wave forcing for tropical upwelling has been substantiated by subsequent works (Plumb and Eluszkiewicz 1999; Butchart and Scaife 2001; Semeniuk and Shepherd 2001; Scott 2002; Eichelberger and Hartmann 2005; Zhou et al. 2006; Geller et al. 2008; Randel et al. 2008; Garcia and Randel 2008; McLandress and Shepherd 2009; Garny et al. 2011; Chen and Sun 2011). Other studies (Boehm and Lee 2003; Kerr-Munslow and Norton 2006; Norton 2006; Ryu and Lee 2010; Garny et al. 2011) indicate that equatorial wave forcing also plays an important role in driving tropical upwelling in the lower stratosphere.

In particular, Ueyama and Wallace (2010) found that tropical upwelling is not significantly correlated with lower-latitude wave forcing on either intraseasonal or interannual time scales, while it is significantly correlated with high-latitude wave forcing on those time scales, thus casting some doubt on the role of lower-latitude wave forcing in driving tropical upwelling that had been established by the previously mentioned works. [This was mentioned in WMO/UNEP (2011, 4.15–4.16) as an issue that needed to be resolved by further research.] Ueyama and Wallace (2010) used both 40-yr European Centre for Medium-Range Weather Forecasts (ECMWF) Re-Analysis (ERA-40) monthly mean and National Centers for Environmental Prediction (NCEP)–National Center for Atmospheric Research (NCAR) (Kalnay et al. 1996) pentad-mean data in their work. Given that a number of authors claim that both transient and stationary waves are important in forcing tropical upwelling, we will see if Ueyama and Wallace's (2010) results still hold when 6-hourly ERA-40 information is used. Also, Ueyama and Wallace (2010) found that the turnaround latitude between tropical upwelling and extratropical downwelling was ~45°, whereas previous authors found the turnaround latitude to be closer to 30°. Given that Ueyama and Wallace (2010) used Microwave Sounding Unit (MSU)–Advanced MSU (AMSU) data, and that the weighting function for these is quite broad in altitude, we will examine the altitude structure of this turnaround latitude.

The remainder of this paper is organized as follows. Section 2 describes the methodology and data used in this study. Section 3 details how the Brewer–Dobson circulation varies in the lower stratosphere. Section 4 demonstrates that both subtropical and tropical wave forcing are important in determining tropical upwelling. Conclusions and discussion are presented in section 5.

2. Methodology and data

Ueyama and Wallace (2010) used both monthly mean data and pentad-mean data to calculate quadratic quantities related to the Eliassen–Palm flux and were unable to find any significant correlation between tropical upwelling and lower-latitude wave forcing. They demonstrated that the meridional eddy heat flux computed from monthly mean ERA-40 data is similar to that calculated from pentad-mean NCEP–NCAR data and concluded that both datasets are reliable and give consistent results. However, in previous studies showing the importance of lower-latitude waves for tropical upwelling, either daily data (Boehm and Lee 2003; Randel

et al. 2008) or 6-hourly data (Kerr-Munslow and Norton 2006) were used to evaluate those quadratic quantities and compile monthly means. Using the downward control principle and ERA-Interim data (Dee et al. 2011) from 1989 to 2008, Garny et al. (2011) recently showed that transient waves and stationary waves contribute comparably to tropical upwelling averaged between 20°S and 20°N at 100 hPa (see their Fig. 4). Randel et al. (2008) also pointed out that transient eddies in both hemispheres over 20°–50° contribute to tropical upwelling. Thus, the abovementioned contradiction might result from missing transient waves in the monthly mean and pentad-mean data used by Ueyama and Wallace (2010).

In this study, the ERA-40 (Uppala et al. 2005) 6-hourly data between 1979 and 2002 are employed because of their length and availability up to the 1-hPa level. The horizontal resolution of the data is 2.5° latitude × 2.5° longitude. Data before 1979 are not used because stratospheric satellite data were not included in the analysis for that period.

Ueyama and Wallace (2010) showed that temporal variations in radiative forcing, except from volcanic eruptions, are strictly seasonal and project almost exclusively onto the equatorial asymmetric component, and determined that the temperature seesaw between the tropics and extratropics projects almost exclusively onto the equatorially symmetric component. In this paper, our approach follows closely that of Ueyama and Wallace (2010). That is to say, empirical orthogonal function (EOF) analysis of the equatorially symmetric component of zonally averaged monthly mean temperature in the lower stratosphere is used to isolate the dominant modes of variability in the BDC.

Since ERA-40 data are on pressure levels, the wave forcing D in (1), the Eliassen–Palm flux $\mathbf{F}$, and its divergence are formulated in pressure coordinates on a sphere as in Andrews et al. (1983):

$$D = \frac{1}{a\cos\varphi}\nabla\cdot\mathbf{F}, \tag{2}$$

$$\mathbf{F} = [F^{(\varphi)}, F^{(p)}] = a\cos\varphi\{-\overline{u'v'} + \psi\overline{u}_p,\ -\overline{u'\omega'} - \psi[(a\cos\varphi)^{-1}(\overline{u}\cos\varphi)_\varphi - f]\}, \tag{3}$$

$$\nabla\cdot\mathbf{F} = (a\cos\varphi)^{-1}\frac{\partial}{\partial\varphi}[F^{(\varphi)}\cos\varphi] + \frac{\partial F^{(p)}}{\partial p}, \tag{4}$$

where

$$\psi = \overline{v'\theta'}/\overline{\theta}_p = -\overline{v'T'}\Big/\left(\frac{\kappa\overline{T}}{p} - \frac{\partial\overline{T}}{\partial p}\right). \tag{5}$$

Here p denotes pressure, (u, v, ω) "velocity" in (longitude, latitude, pressure) coordinates, θ potential temperature, T temperature, f the Coriolis parameter, and κ the ratio of the gas constant to the specific heat at constant pressure. Primes denote departures from the zonal means, which are represented by overbars, and all other notations are as commonly used (Andrews et al. 1987).

In this paper, wave forcing D in (2) is calculated via 6-hourly data and collected into its monthly mean value for analysis in order to properly account for both stationary and transient waves. Randel et al. (2004) have shown that differences exist among various stratospheric datasets. Discrepancies are shown in the primary observed variables (i.e., winds and temperatures), and these differences become larger for quadratics of these primary quantities (i.e., heat and momentum fluxes). The Eliassen–Palm fluxes involve these quadratic terms, and the wave forcing involves differences in derivatives of these quadratic fluxes [see (2)–(5)]. Furthermore, these differences between quadratic quantities involve a great deal of cancellation between terms, so the wave forcing is very difficult to determine accurately from reanalysis data. Geller et al. (2008) and others have shown that close to the equator, small divergences of the Eliassen–Palm flux become increasingly important. Also, $F^{(p)}$ associated with vertical eddy fluxes $\overline{u'\omega'}$ in the tropics has significant contribution from gravity waves, some of which are likely not well resolved in the ERA-40 (e.g., Bergman and Salby 1994; Giorgetta et al. 2002, Watanabe et al. 2008). Thus, the accuracy of the calculated EP flux divergences is further limited in the deep tropics.

To test the statistical significance of the correlation coefficients $r(x, y)$ between the BDC and wave forcings, we use the methodology adopted by Oort and Yienger (1996) as follows. We use the null hypothesis that the population value $\rho(x, y) = 0$. The confidence limits were calculated via Fisher's Z transformation (Spiegel et al. 2008):

$$Z = \frac{1}{2}\ln\left[\frac{1 + r(x,y)}{1 - r(x,y)}\right]. \tag{6}$$

The Z statistic is approximately normally distributed with a mean value

$$\mu_z = \frac{1}{2}\ln\left[\frac{1 + \rho(x,y)}{1 - \rho(x,y)}\right] \quad (7)$$

and a standard deviation

$$\sigma_z = \frac{1}{\sqrt{N_{\rm df} - 3}}, \quad (8)$$

where $N_{\rm df}$ is the number of degrees of freedom, which is given by Oort and Yienger (1996):

$$N_{\rm df} = N\left[1 + \frac{2}{N}\sum_{\tau=1}^{N-1}(N-\tau)r_\tau(x)r_\tau(y)\right]^{-1}. \quad (9)$$

Here, N is the sample size, and $r_\tau(x)$ and $r_\tau(y)$ are the autocorrelation coefficients at lag τ.

3. Variations of the Brewer–Dobson circulation

Ueyama and Wallace (2010) demonstrated that the temperature seesaw between the tropics and extratropics is almost entirely captured by the even (equatorially symmetric) component of the meridional temperature distribution, defined as the mean of zonally averaged temperatures at corresponding latitudes in the Northern and Southern Hemisphere, $(T_{\rm NH} + T_{\rm SH})/2$. To exclude the contribution of volcanic eruptions and the long-term cooling trend to the interannual variability (Ueyama and Wallace 2010), the global mean temperatures are subtracted from the meridional temperature distributions. The resultant meridional temperature distributions are further processed, with their climatological annual mean distribution (i.e., averaged over 264 months between January 1980 and December 2001) further removed to highlight the temperature seesaw structure associated with the variability of wave forcing. A standard EOF analysis is performed on these anomaly distributions weighted by the square root of the cosine of the midpoint latitude for each zonal belt in order to analyze area-weighted variances. Henceforth, we refer to the weighted anomaly distributions as T^*. Note that the data in 1979 and 2002 are only used to construct the low-pass filtered fields for studying the interannual variability, which in turn are employed to obtain the high-pass filtered fields for studying the intraseasonal variability.

To better understand the temporal and spatial variations in the BDC, we mimic the lower-stratospheric brightness temperatures (hereafter referred as to T_b) of the MSU–AMSU by applying the weighting function of the lower-stratospheric channel of the MSU–AMSU to the ERA-40 temperature fields:

$$T_b = W_s T(0) + \int_0^{\rm TOA} W(z)T(z)\,dz, \quad (10)$$

where W_s is the surface weight, $T(z)$ the temperature at height z, and $W(z)$ the temperature weighting function, and the integral extends from the surface to the top of the atmosphere (TOA) (Mears and Wentz 2009). The $W(z)$ of the lower-stratospheric channel is concentrated mainly in the 30–150 layer, which is available online (from www.ssmi.com/msu) and shown in Fueglistaler et al. (2011; see their Fig. 3). For the calculation of T_b in (10), we use cubic spline interpolation to obtain the temperatures at the levels where the values of the weighting function are available.

For T_b^*, the three largest eigenvalues account for 92.7%, 4.5%, and 1.7% of the total month-to-month variance whereas Ueyama and Wallace (2010) indicated that EOF 1 accounts for 93% of the variance using MSU/AMSU data. Figure 1 shows the first leading EOF and time series of its coefficient. The first leading EOF pattern clearly represents the temperature seesaw associated with variations of the BDC—that is, the BDC in the lower stratosphere is strongest in the boreal winter and weakest in the boreal summer—which is consistent with the results of Yulaeva et al. (1994), among others. The turnaround latitude in Fig. 1a is approximately 43.75°; Ueyama and Wallace (2010) found the crossing latitude to be ~45° using MSU–AMSU data. Combining EOF 1 and the corresponding first principal component (PC) in Fig. 1, we can infer that our mimicked equatorial brightness temperatures in the lower stratosphere are above the climatological annual mean by about 2°C during boreal summers with maxima in July/August, and below the climatological annual mean by about 2°C during boreal winters with minima in January/February, which are comparable to the results of Ueyama and Wallace (2010). Therefore, EOF 1 and PC 1 derived from our mimicked brightness temperatures via ERA-40 data depict almost identical properties of the BDC to those revealed by Ueyama and Wallace (2010) using MSU–AMSU data. In the remaining parts of this section, we will investigate how the temperature seesaw associated with variations of the BDC changes with altitude in the lower stratosphere.

For T^* at the 70-hPa level, the three largest eigenvalues account for 90.1%, 5.1%, and 3.1% of the total month-to-month variance. Figure 2 shows the first leading EOF and time series of its coefficient. The first leading EOF pattern at the 70-hPa level is similar to that shown in Fig. 1. However, the turnaround latitude in Fig. 2a is approximately 37.5°, which is comparable to the value derived from the Met Office (UKMO) analysis and the results from various GCMs (Butchart et al. 2006, see their Figs. 1 and 2), whereas Ueyama and Wallace (2010) found the crossing latitude to be ~45° using MSU–AMSU data. Combining EOF 1 and

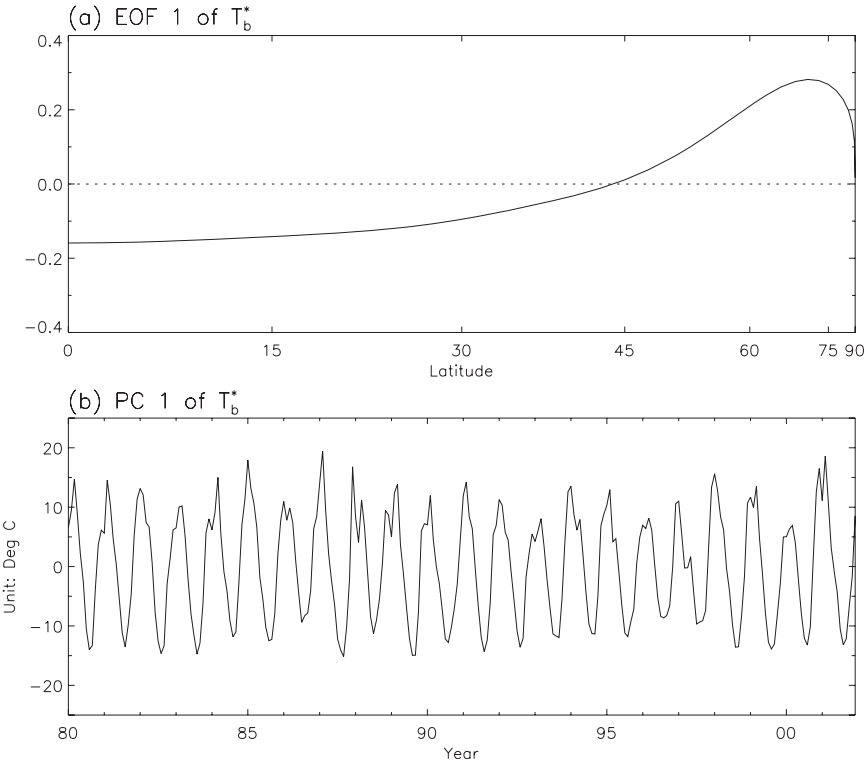

FIG. 1. (a) The first leading EOF of T_b^* from 1980 to 2001 and (b) the corresponding first principal component time series. The horizontal scale in (a) is such that the spacing between latitudes is proportional to the area of the earth's surface between them (i.e., is linear in the sine of the latitude) (Gill 1982).

the corresponding first PC in Fig. 2, we can infer that equatorial temperatures are above the climatological annual mean by about 2°–4°C during boreal summers with maxima in July/August, and below the climatological annual mean by about 2°–4°C during boreal winters with minima in January/February, indicating that the amplitudes of the annual cycles in equatorial temperatures at 70 hPa are larger than those of the equatorial temperatures derived from the MSU/AMSU data (~2°C) by Ueyama and Wallace (2010). Figure 2 also shows that the amplitude of the temperature seesaw exhibits strong interannual variability. For instance, the minimum equatorial temperature that occurred in February 2000 is slightly less than 2°C below the climatological annual mean whereas that in January 1998 is nearly 5°C below the climatological annual mean. In addition, PC 1 shows appreciable intraseasonal variability during northern winters due to the stratospheric vacillations (Holton and Mass 1976; Yoden 1987) associated with the stronger wave forcings in those seasons.

Similar EOF analysis is further performed on T^* at the 150- and 30-hPa levels to understand why the turnaround latitude and the amplitudes of the annual cycles shown in Fig. 2 differ from those shown in Ueyama and Wallace (2010) where the EOF analysis is performed on the MSU/AMSU deep-layer atmospheric temperatures rather than the temperatures at any individual pressure level. For T^* at the 150-hPa level, the three largest eigenvalues account for 86.9%, 7.1%, and 3.7% of the total month-to-month variance. Figure 3 shows the first leading EOF and time series of its coefficient at the 150-hPa level. Although the first leading EOF pattern also shows the temperature seesaw structure at the 150-hPa level, the turnaround latitude at that level is about 51° while the amplitudes of the annual cycles can be inferred as only about 1°C in the equatorial regions. For T^* at the 30-hPa level, the three largest eigenvalues account for 75.5%, 17.1%, and 5.8% of the total month-to-month variance. Figure 4 shows the first leading EOF and time series of its coefficient at the 30-hPa level. The first leading EOF pattern at the 30-hPa level again represents the temperature seesaw between low latitudes and high latitudes. Both the turnaround latitude and the amplitudes of the annual cycles are comparable to those in Ueyama and Wallace (2010).

We also performed the EOF analysis on T^* at the 50- and 100-hPa levels. The three largest eigenvalues at the 50-hPa level account for 86.9%, 7.3%, and 3.9% of

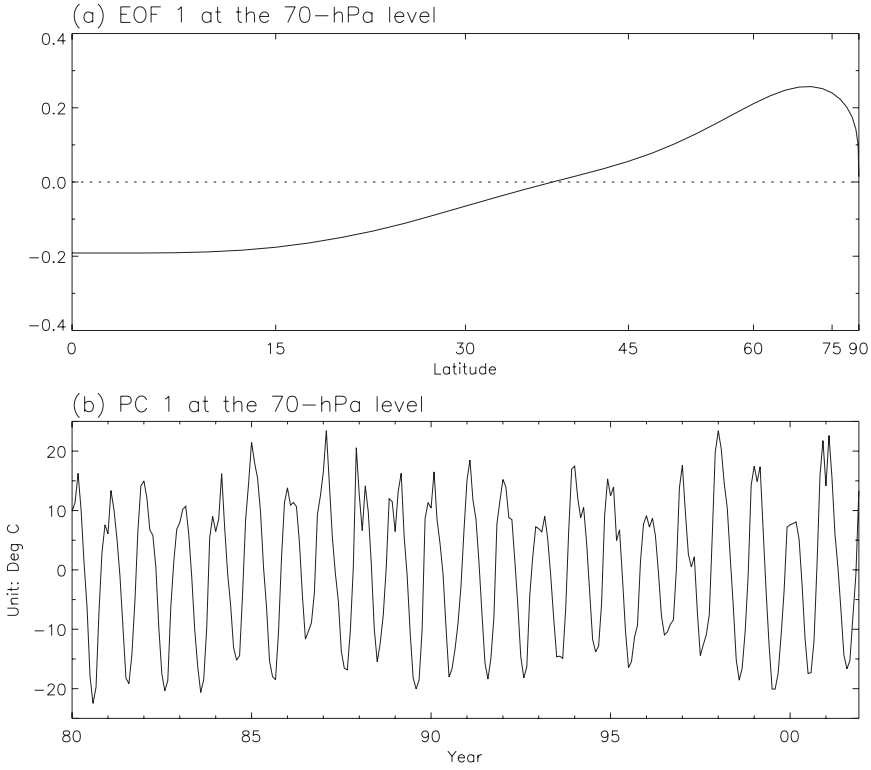

FIG. 2. As in Fig. 1, but for T^* at the 70-hPa level from 1980 to 2001.

the total month-to-month variance while those eigenvalues at the 100-hPa level account for 88.3%, 6.7%, and 3.2% of the variance. The first leading EOF pattern and PC at either level (not shown) are also similar to those shown in Fig. 1. The turnaround latitudes are approximately 42.5° and 46° at the 50- and 100-hPa levels, respectively. These first leading EOF patterns and PCs also indicate that the BDC in the lower stratosphere is strongest in the boreal winter and weakest in the boreal summer. The amplitudes of the annual cycles are 1.5°–3°C at the 50-hPa level and 2°–3°C at the 100-hPa level in the equatorial regions.

Reed and Vlcek (1969) showed that the annual temperature variation in the lower tropical stratosphere has its maximum amplitude at the 80-hPa level. It follows that the amplitudes of the annual cycles in the equatorial temperatures at the 70-hPa level shown in Fig. 2 are larger than those at the 150-, 100-, 50-, and 30-hPa levels. Consequently, the annual temperature variation at the 70-hPa level has larger amplitude than that for the 30–150-hPa layer shown by Ueyama and Wallace (2010) and in Fig. 1.

The turnaround latitude at the 70-hPa level shown in Fig. 2 is located equatorward of that at the 50-hPa level (42.5° latitude; not shown), which is in turn located equatorward of that at the 30-hPa level shown in Fig. 4. These results are consistent with previous studies (Butchart et al. 2006; McLandress and Shepherd 2009; Simpson et al. 2011; Chen and Sun 2011) indicating that the turnaround latitude shifts poleward with increasing height below 30 hPa in the lower stratosphere. We also found that the turnaround latitude at the 70-hPa level shown in Fig. 2 is located equatorward of that at the 100-hPa level (46° latitude; not shown), which is in turn located equatorward of that at the 150-hPa level shown in Fig. 3. The turnaround latitudes shown in Figs. 2–4 are consistent with the result of Ueyama and Wallace (2010) and that shown in Fig. 1. For T^* at the 30-hPa level, the first eigenvalue only accounts for 75.5% of the total month-to-month variance while the first eigenvalues at the 70- and 150-Pa levels account for 90.1% and 86.9% of the variances respectively, indicating that although the annual variation is still a dominant dynamical mode of the BDC at the 30-hPa level, other dynamical modes also play a role at this level. Since the second and third eigenvalues at the 30-hPa level account for 17.1% and 5.8% respectively, the second EOF at the 30-hPa level is physically relevant according to North's rule of thumb (North et al. 1982). Figure 5 shows the second leading EOF and time series of its coefficient for T^* at the 30-hPa level. EOF 2 in Fig. 5a shows a tripolar structure with a negative–positive–negative structure with

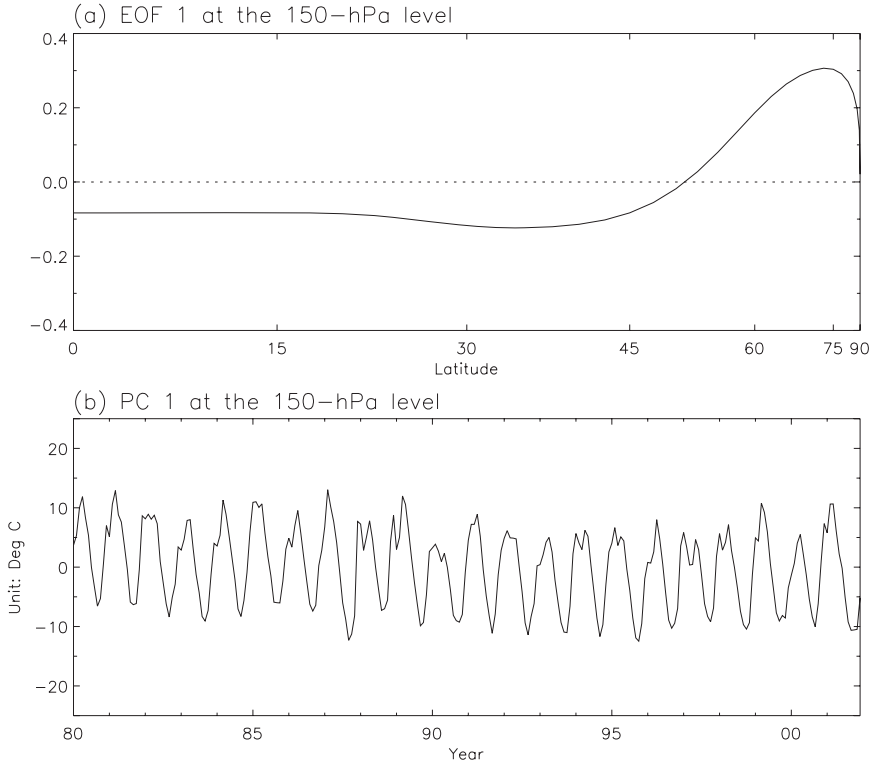

FIG. 3. As in Fig. 1, but for T^* at the 150-hPa level from 1980 to 2001.

increasing latitude. The lower-latitude seesaw in Fig. 5a depicts the anticorrelation between equatorial and subtropical/extratropical temperatures at the 30-hPa level. This latitudinal temperature gradient is associated with the vertical shear of the zonal mean zonal wind at that level as shown in Fig. 5b, due to the thermal wind relationship. PC 2 in Fig. 5b shows that the second dynamical mode is dominated by the quasi-biennial oscillation (QBO). Combining EOF 2 and the corresponding PC 2 in Fig. 5, we can infer that the amplitudes of equatorial temperature QBO are about 4°C, which is comparable to those derived from the UKMO analyses by Randel et al. (1999b, see their Fig. 2). Since the QBO is most prominent between 5 and 40 hPa (Baldwin et al. 2001), EOF 1, which is dominated by annual variations, only accounts for 75.5% of the total month-to-month variance at the 30-hPa level whereas it accounts for ~90% of the total month-to-month variance at the 70- and 150-hPa levels. This low-latitude temperature seesaw was first deduced by Reed (1964, see his Fig. 8). It is associated with the QBO-induced meridional circulation envisaged by Reed (1964) and simulated by Plumb and Bell (1982). The high-latitude seesaw in Fig. 5a depicts the anticorrelation between middle-latitude and polar temperatures at the 30-hPa level, and is largely ascribed to the finding by Labitzke (1982) that the 30-hPa polar vortex poleward of 55°N is much colder when the 50-hPa equatorial winds (see Fig. 5b) are from the west as per the Holton–Tan (Holton and Tan 1980, 1982) mechanism. The tripolar structure shown in Fig. 5a confirms the finding by Ruzmaikin et al. (2005) that the mechanism of the QBO influence on the extratropics operates mostly through the modulation of the northern annular mode (Thompson and Wallace 2000), However, the QBO influence on the winter polar vortex is an unsettled and complicated issue (Wallace and Chang 1982; Dunkerton and Baldwin 1991; Gray et al. 2004; Naoe and Shibata 2010; Powell and Xu 2010), and further discussion on this is beyond the scope of this paper.

In summary, in this section we have shown that the leading mode of variability in the BDC between the 150- and 30-hPa levels is dominated by the annual cycle with extrema in January/February and July/August, and that the turnaround latitude of the BDC varies with altitude. In addition, the BDC exhibits both intraseasonal and interannual variability.

4. Relationship of the BDC to wave forcing

Many studies have established that wave forcing at lower latitudes plays a crucial role in driving the tropical upwelling portion of the Brewer–Dobson circulation

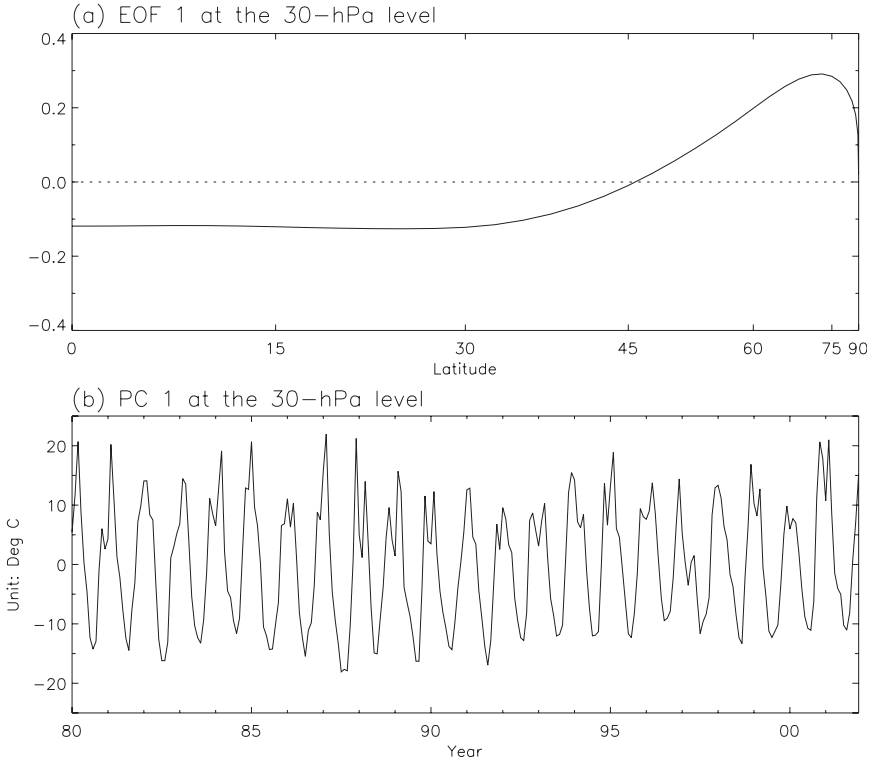

FIG. 4. As in Fig. 1, but for T^* at the 30-hPa level from 1980 to 2001.

(Plumb and Eluszkiewicz 1999; Semeniuk and Shepherd 2001; Scott 2002; Eichelberger and Hartmann 2005; Zhou et al. 2006; Geller et al. 2008; Randel et al. 2008; Garcia and Randel 2008; Garny et al. 2011; Chen and Sun 2011). Ueyama and Wallace (2010) argued that if the lower-latitude wave forcing does play an important role in the annual cycle in the BDC as per those previous studies, then the nonseasonal variability in the EP fluxes might force some of the nonseasonal variability in the BDC as well. Using pentad NCEP–NCAR data and monthly mean ERA-40 data, Ueyama and Wallace (2010) found that the nonseasonal variability in the BDC is not significantly correlated with that in lower-latitude wave forcing. In this section, we show that nonseasonal variabilities in the BDC and the lower-latitude wave forcing are indeed significantly correlated if 6-hourly ERA-40 data are employed, thus properly taking transient waves into account.

It is pointed out in section 2 that the accuracy of the calculated EP flux divergences is very limited in the deep tropics. In addition, the downward control principle is not applicable in the deep tropics because the gradient of angular momentum [i.e., $\overline{m}_\varphi$ in (1)] tends to vanish there (Haynes et al. 1991). Thus, we only present how the BDC is correlated to wave forcings between 15° and 85° latitude where (1) can be approximated (Haynes et al. 1991) by

$$\overline{w}^*(\varphi, z) = -\frac{1}{\rho_0 a \cos\varphi}\frac{\partial}{\partial\varphi}\left[\frac{\cos\varphi}{2\Omega\sin\varphi}\int_z^\infty (\rho_0 D)_{\varphi=\text{const}}\, dz'\right]. \tag{11}$$

Combining (2) and (11) leads to

$$\overline{w}^*(\varphi, z) = -\frac{1}{\rho_0 g a^2 \cos\varphi}\frac{\partial}{\partial\varphi}\left[\frac{1}{2\Omega\sin\varphi}\int_0^p (\mathbf{V}\cdot\mathbf{F})_{\varphi=\text{const}}\, dp'\right], \tag{12}$$

where g is the acceleration of gravity and other symbols are described in previous sections.

Similarly to Rosenlof (1995) and Butchart et al. (2006), the 70-hPa level is selected to represent the lower stratosphere for purpose of investigating the BDC. The corresponding wave forcing at each parallel is measured by

$$\text{WF} = \int_{p_1}^{p_2} (\mathbf{V}\cdot\mathbf{F})_{\varphi=\text{const}}\, dp, \tag{13}$$

where $p_1 = 1$ hPa and $p_2 = 70$ hPa.

The wave forcing term WF in (13) is widely used to estimate tropical upwelling in the lower stratosphere (Butchart et al. 2006, 2010, 2011; Shepherd and McLandress 2011; Garny et al. 2011; Chun et al. 2011).

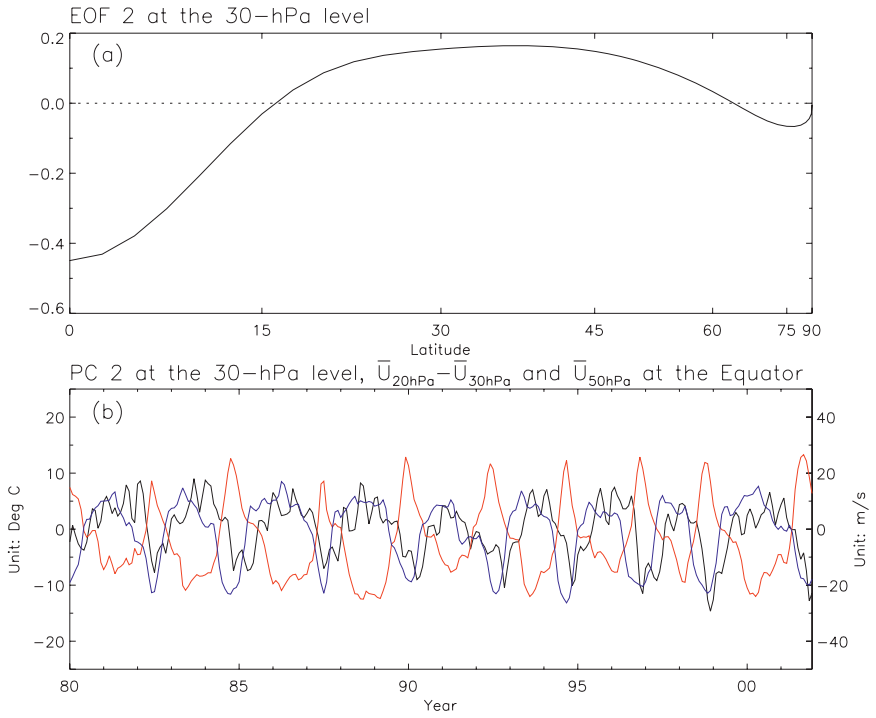

FIG. 5. (a) The second leading EOF of T^* at the 30-hPa level from 1980 to 2001. The horizontal scale is as in Fig. 1a. (b) The corresponding second principal component time series (black line), the vertical shear of the zonal mean equatorial zonal wind at the 30-hPa level represented by $\overline{u}_{20\,\mathrm{hPa}} - \overline{u}_{30\,\mathrm{hPa}}$ (red line), and the zonal mean equatorial zonal wind at the 50-hPa level (blue line).

The total upwelling mass flux across an isobaric surface within $[-\varphi_0, \varphi_0]$ latitudes, $F_m^{\uparrow}$, is obtained by the total compensating downwelling mass flux outside $[-\varphi_0, \varphi_0]$ latitudes:

$$F_m^{\uparrow} = -\left(\int_{-\pi/2}^{-\varphi_0} 2\pi a\rho_0 \overline{w}^* \cos\varphi \, d\varphi + \int_{\varphi_0}^{-\pi/2} 2\pi a\rho_0 \overline{w}^* \cos\varphi \, d\varphi\right). \quad (14)$$

Combining (12), (13), and (14) leads to

$$F_m^{\uparrow} = -\frac{\pi}{g\Omega a \sin\varphi_0}(\mathrm{WF}|_{\varphi=-\varphi_0} + \mathrm{WF}|_{\varphi=\varphi_0}), \quad (15)$$

which indicates that total upwelling mass flux within $[-\varphi_0, \varphi_0]$ latitudes is determined by the sum of wave forcing at $-\varphi_0$ and φ_0.

To elucidate how wave forcing in the polar regions plays a role in the temperature seesaw structures discussed in section 3, the total downward mass flux across an isobaric surface in both $[-\varphi_p, -\varphi_0]$ and $[\varphi_0, \varphi_p]$ latitudes is given as follows:

$$F_m^{\downarrow} = \int_{-\varphi_p}^{-\varphi_0} 2\pi a\rho_0 \overline{w}^* \cos\varphi \, d\varphi + \int_{\varphi_0}^{\varphi_p} 2\pi a\rho_0 \overline{w}^* \cos\varphi \, d\varphi, \quad (16)$$

where φ_p is a polar latitude less than $\pi/2$.

Combining (12), (13), and (16) yields

$$F_m^{\downarrow} = \frac{\pi}{g\Omega a}\left(\frac{\mathrm{WF}|_{\varphi=-\varphi_0} + \mathrm{WF}|_{\varphi=\varphi_0}}{\sin\varphi_0} - \frac{\mathrm{WF}|_{\varphi=-\varphi_p} + \mathrm{WF}|_{\varphi=\varphi_p}}{\sin\varphi_p}\right), \quad (17)$$

which demonstrates that the magnitude of the total downward mass flux in both $[-\varphi_p, -\varphi_0]$ and $[\varphi_0, \varphi_p]$ latitudes (i.e., $-F_m^{\downarrow}$) is negatively correlated with the sum of the wave forcing at $-\varphi_0$ and φ_0, and positively correlated with the sum of the wave forcing at $-\varphi_p$ and φ_p.

Geller et al. (2008) pointed out that tropical upwelling in the BDC is not sensitive to the wave forcing in the polar regions, which is consistent with (15). However, (17) reveals that the wave forcing in the polar regions is

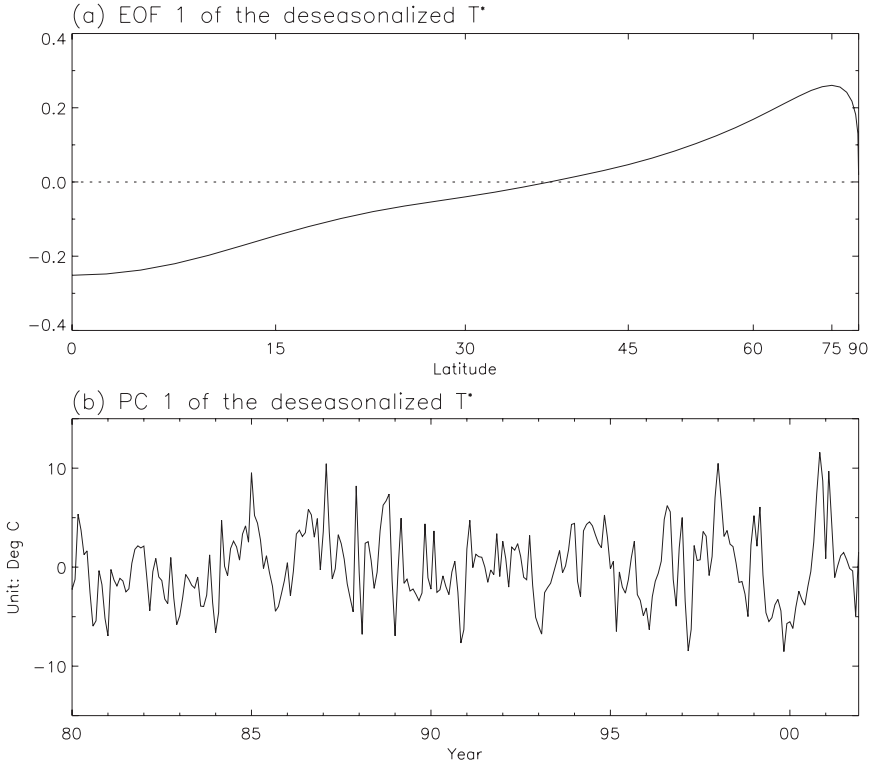

FIG. 6. (a) The first leading EOF of the deseasonalized T^* at the 70-hPa level from 1980 to 2001 and (b) the corresponding first principal component time series. The horizontal scale in (a) is as in Fig. 1a.

important in determining the latitudinal structure of Brewer–Dobson downwelling.

a. Nonseasonal variabilities of the lower stratospheric BDC and wave forcing

To investigate nonseasonal variabilities of the lower stratospheric BDC and wave forcing, the climatological mean annual cycles over the period 1980–2001 are further removed from T^* at the 70-hPa level. The corresponding wave forcing [WF expressed in (13)], is treated in the same manner, so that associations between the deseasonalized T^* at the 70-hPa level and the deseasonalized WF can be investigated.

An EOF analysis was performed on the deseasonalized T^* at the 70-hPa level. The largest eigenvalue accounts for 57.5% of the total month-to-month variance. Figure 6 shows the first leading EOF and time series of its coefficient. The first leading EOF pattern still represents the temperature seesaw associated with nonseasonal variations of the BDC in the lower stratosphere with its turnaround latitude located near 37.5°, which is ~10° equatorward of that derived by Ueyama and Wallace (2010). As indicated earlier, their value represents the mean crossing latitude over the 30–150-hPa layer. PC 1 and EOF 1 in Fig. 6 indicate that the amplitudes of the nonseasonal variations in equatorial temperatures at the 70-hPa layer are very irregular with the maximum amplitude being ~3°C.

Figure 7 shows the latitudinal distribution of the contemporary correlation coefficients between the PC 1 of the deseasonalized T^* at the 70-hPa level and the deseasonalized WF expressed in (13). Figure 7a illustrates that the wave forcing between 17.5° and 65° latitude coherently, significantly, and negatively correlates with PC 1 at the 95% confidence level when 6-hourly ERA-40 data are used. However, Fig. 7b shows that wave forcing in the subtropics no longer significantly correlates with the PC 1 at the 95% confidence level when monthly mean ERA-40 data are used even though the wave forcing between 42.5° and 67.5° latitude still significantly correlates with the PC 1 at the 95% confidence level.

Figure 7 shows that the PC1 are negatively and significantly correlated with wave forcings between 42.5° and 65° latitude no matter what kind of dataset is used, which confirms the importance of planetary-wave breaking in the stratospheric "surf zone" (McIntyre and Palmer 1983, 1984) to the BDC. Figure 7b is also largely consistent with the results of Ueyama and Wallace (2010), namely that

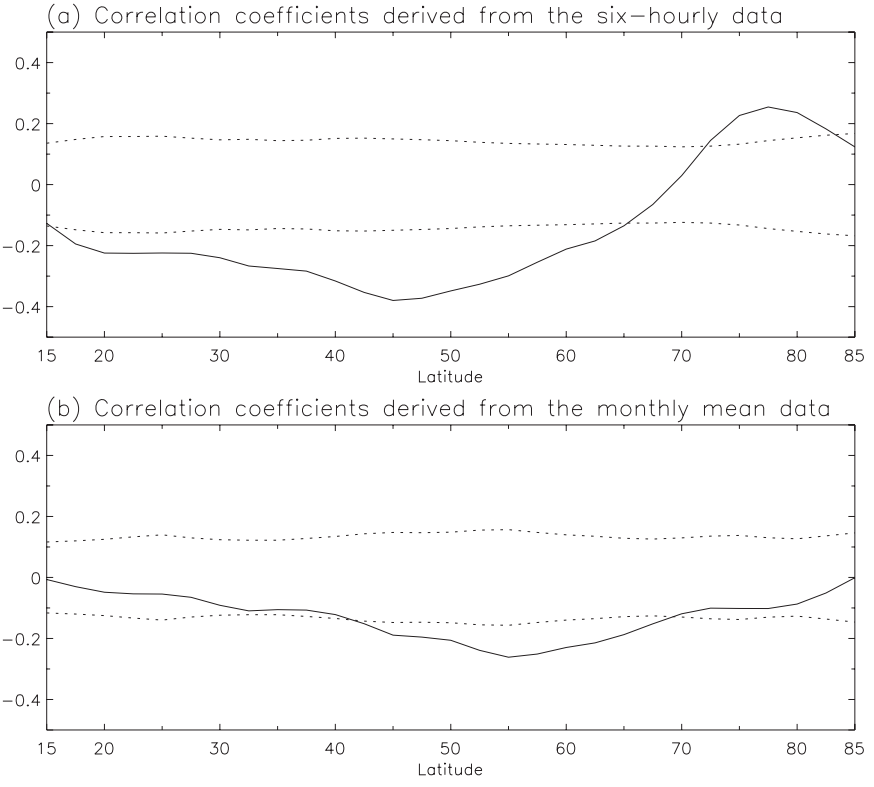

FIG. 7. Contemporary correlation coefficients (solid line) between PC 1 of the deseasonalized T^* at the 70-hPa level and the deseasonalized wave forcings from 1980 to 2001 derived from (a) the 6-hourly ERA-40 data and (b) the monthly mean ERA-40 data. Dotted lines denote the 95% confidence limits as a function of latitude.

tropical upwelling in the BDC is significantly correlated with the high-latitude wave forcing. Contrary to Ueyama and Wallace (2010), however, Fig. 7a clearly demonstrates that subtropical wave forcing plays an important role in driving the tropical upwelling portion of the Brewer–Dobson circulation as shown by Plumb and Eluszkiewicz (1999), Zhou et al. (2006), Geller et al. (2008), and Chen and Sun (2011).

Figure 7a also shows that the PC1 is positively and significantly correlated with wave forcings between 72.5° and 82.5° latitude, which is consistent with the above-mentioned conclusion drawn from (17). However, this feature is not shown in Fig. 7b where transient waves are not included.

Note that, in this figure, our correlations are less than shown in Ueyama and Wallace's (2010) Table 2a. This is because of some differences in our calculations. Ueyama and Wallace consider $\overline{v'T'}$ as their wave forcing, while we consider the divergence of the Eliassen–Palm flux as our wave forcing. Ueyama and Wallace's (2010) correlations are based on their wave forcing weighted between one month before and during the same month as their EOF, such that their correlations are maximized. Our correlations are for the same months of the wave forcing and the EOF. We have examined the correlations between our wave forcing one month before the EOF, and our correlations increase substantially to values that approach, but are still less than those shown by Ueyama and Wallace (2010). Presumably, we could make these correlations approach those of Ueyama and Wallace (2010) even more closely if we maximized our weighting as they did, but we have not done so, since there would still be the differences in wave forcing to consider.

b. *Interannual variabilities of the lower stratospheric BDC and wave forcing*

To investigate interannual variabilities of the lower stratospheric BDC and wave forcing, we further apply successively centered five- and three-month running mean smoothing operators to the deseasonalized T^* at the 70-hPa level and the deseasonalized wave forcing to form the low-pass filtered version (Ueyama and Wallace 2010). Figure 8a shows EOF 1 of the low-pass filtered and deseasonalized T^*, which accounts for 58.2% of the total month-to-month variance. In the low-pass filtered

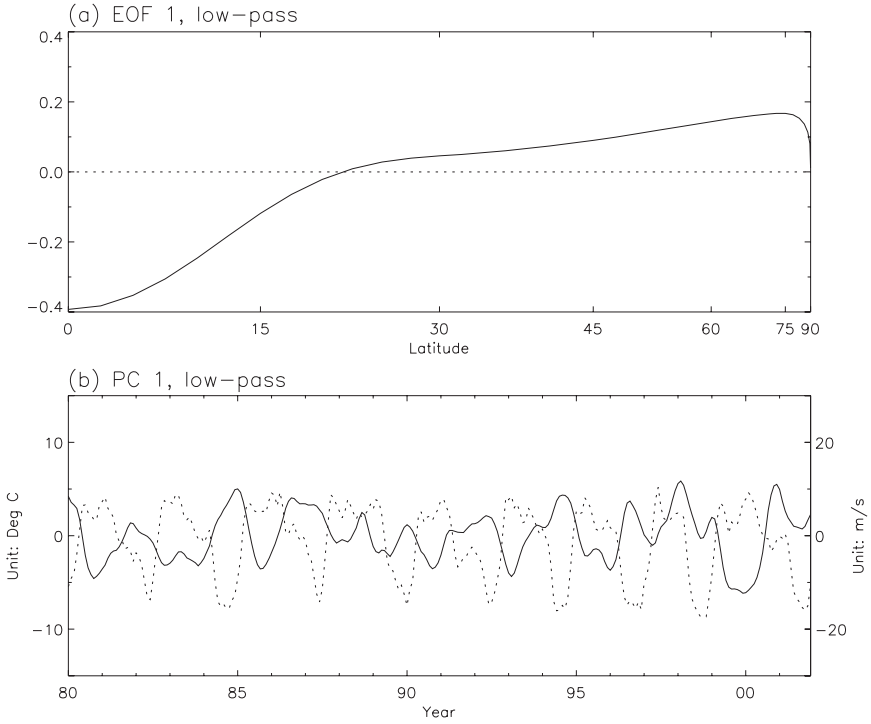

FIG. 8. (a) The first leading EOF of the low-pass filtered and deseasonalized T^* at the 70-hPa level from 1980 to 2001. The horizontal scale is as in Fig. 1a. (b) The corresponding first principal component (solid line) and the vertical shear of the zonal mean equatorial zonal wind at the 70-hPa level represented by $\overline{u}_{50\,\mathrm{hPa}} - \overline{u}_{70\,\mathrm{hPa}}$ (dotted line).

pattern, the crossing latitude is located near 22.5°, which is ~15° equatorward of the mean crossing latitude over the 30–150-hPa layer derived by Ueyama and Wallace (2010). PC 1 and EOF 1 in Fig. 8 indicate that the amplitude of the interannual variations in equatorial temperatures at the 70-hPa level is about 2°C. PC 1 exhibits an apparent QBO variation. Figure 8b shows that PC 1 is negatively correlated with the vertical shear of the zonal mean equatorial zonal wind at the 70-hPa level represented by $\overline{u}_{50\,\mathrm{hPa}} - \overline{u}_{70\,\mathrm{hPa}}$. The contemporary correlation coefficient is −0.57. The degrees of freedom are 16. Thus, the two-tailed test verifies that the vertical shear and PC 1 are significantly correlated at the 95% confidence level.

Using the QBO index—that is, the time series of the vertical shear of the zonal mean equatorial zonal wind at the 70-hPa level shown in Fig. 8b—we remove the QBO signal from the low-pass filtered and deseasonalized T^* via the linear regression method to obtain the QBO-residual T^*. EOF 1 of the QBO-residual T^* accounts for 65.5% of the total month-to-month variance. The crossing latitude is located near 32.8° (not shown), which is only ~5° equatorward of the mean crossing latitude over the 30–150-hPa layer derived by Ueyama and Wallace (2010), indicating that the QBO-induced meridional circulation (Reed 1964; Plumb and Bell 1982) plays an important role on the interannual time scale.

Figure 9 shows the latitudinal distribution of the contemporary correlation coefficients between the PC 1 of the low-pass filtered and deseasonalized T^* at the 70-hPa level and the low-pass filtered and deseasonalized WF expressed in (13). Figure 9a demonstrates that wave forcing between 20° and 62.5° latitude coherently, significantly, and negatively correlates with PC 1 at 95% confidence level when 6-hourly ERA-40 data are used. However, Fig. 9b shows that wave forcing in the subtropics no longer significantly correlates with the PC 1 at 95% confidence level when monthly mean ERA-40 data are used even though wave forcing around 45° and 65° latitude respectively still significantly correlates with the PC 1 at the 95% confidence level. Thus, we conclude that subtropical wave forcing does play an important role in driving the tropical upwelling portion of the Brewer–Dobson circulation on interannual time scale when the contributions from transient waves are considered.

Salby (2011) pointed out that the variation of wave forcing alone cannot reproduce the observed response of stratospheric temperature and ozone in his model, and that nearly all of the interannual variance of stratospheric

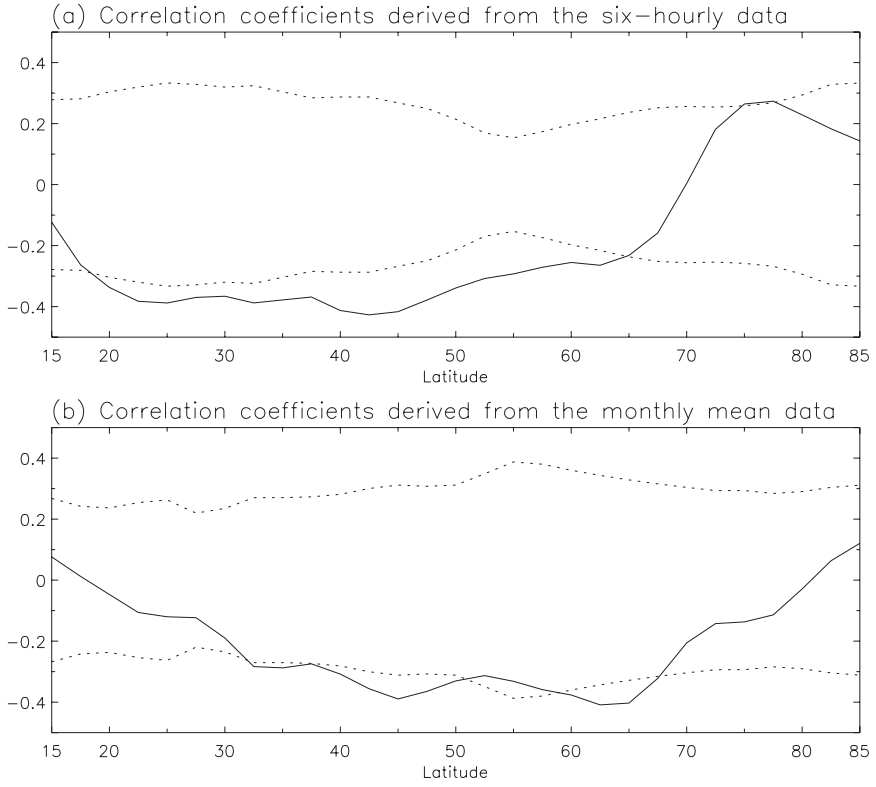

FIG. 9. As in Fig. 7, but for the low-pass filtered and deseasonalized T^* at the 70-hPa level and the corresponding wave forcing.

temperature and ozone over the Northern Hemisphere can be explained if both the variation of wave forcing and the stratospheric QBO of equatorial wind are included.

c. *Intraseasonal variabilities of the lower stratospheric BDC and wave forcing*

To investigate intraseasonal variabilities of the lower stratospheric BDC and wave forcing, we subtract the low-pass filtered and deseasonalized T^* at the 70-hPa level and the corresponding wave forcing from the deseasonalized T^* and wave forcing respectively. Figure 10a shows EOF 1 of the high-pass filtered and deseasonalized T^*, which accounts for 76.0% of the total month-to-month variance. In the high-pass filtered pattern, the crossing latitude is located near 47.5°, which is roughly the same as the mean crossing latitude (i.e., 50°) over the 30–150-hPa layer derived by Ueyama and Wallace (2010). In addition, the pattern is also characterized by remarkably uniform amplitudes equatorward of the crossing latitude and much larger temperature anomalies of opposite sign in the polar region as pointed out by Ueyama and Wallace (2010). PC 1 and EOF 1 in Fig. 10 indicate that that the amplitudes of the intraseasonal variations in equatorial temperatures at the 70-hPa level are very irregular with the maximum amplitude being ~1°C.

Figure 11 shows the latitudinal distribution of the contemporary correlation coefficients between the PC 1 of the high-pass filtered and deseasonalized T^* at the 70-hPa level and the high-pass filtered and deseasonalized WF expressed in (13). Figure 11a demonstrates that the wave forcing between 27.5° and 62.5° latitude coherently, significantly, and negatively correlates with PC 1 at the 95% confidence level when 6-hourly ERA-40 data are used. Figure 11b shows that only wave forcing between 55° and 65° latitude is significantly correlated with PC 1 at the 95% confidence level when monthly mean ERA-40 data are used.

In addition, Fig. 11a shows that the PC1 are positively and significantly correlated with wave forcings between 75° and 82.5° latitude, which is similar to the result shown in Fig. 7a. However, this feature does not appear in Fig. 11b where only stationary waves are included.

Equations (1) and (12) are only valid in the steady state (Haynes et al. 1991). Rosenlof and Holton (1993) indicated that application of the ''downward control'' principle appears to only be valid for the solstice seasons. They pointed out that the assumption of steady state is violated in the equinox seasons, leading to an

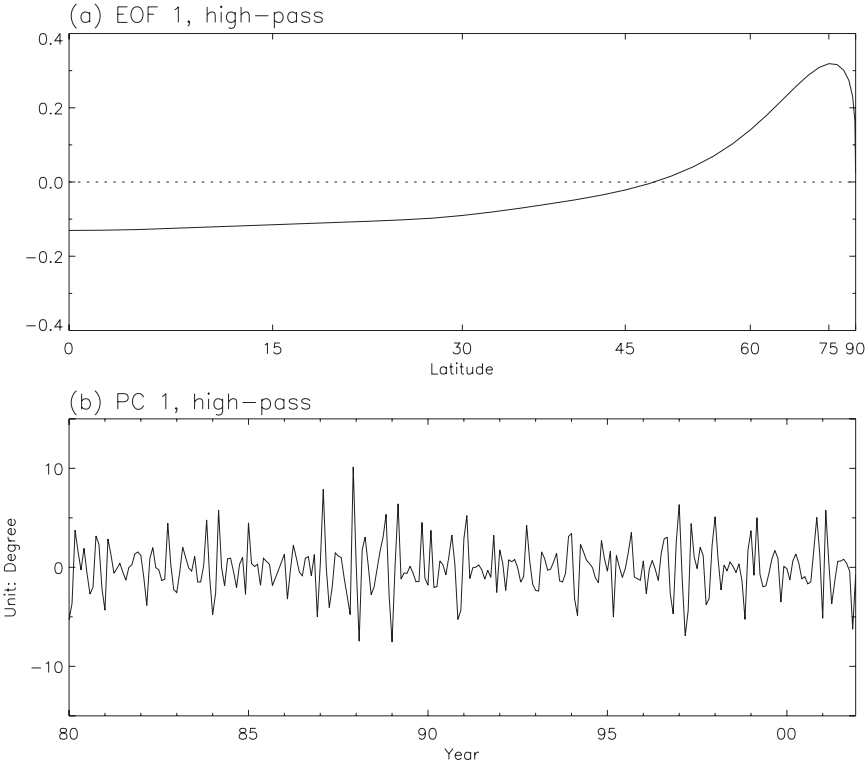

FIG. 10. As in Fig. 1, but for the high-pass filtered and deseasonalized T^* at the 70-hPa level.

inaccurate estimate of the residual circulation streamfunction during those seasons if the downward control principle is employed. Since wave forcing drives the mean meridional circulation and accelerates the zonal mean zonal wind on intraseasonal time scales, the downward control principle (1) can be modified as follows (Randel et al. 2002, 2008):

$$\overline{w}^*(\varphi, z) = \frac{1}{\rho_0 \cos\varphi}\frac{\partial}{\partial\varphi}\left\{\int_z^\infty \left[\frac{\rho_0 a\left(D - \dfrac{\partial\overline{u}}{\partial t}\right)\cos^2\varphi}{\overline{m}_\varphi}\right]_{\overline{m}=\text{const}} dz'\right\}. \tag{18}$$

The modified version of (12) can be written as

$$\overline{w}^*(\varphi, z) = -\frac{1}{\rho_0 g a^2 \cos\varphi}\frac{\partial}{\partial\varphi} \times\left[\frac{1}{2\Omega\sin\varphi}\int_0^p \left(\nabla\cdot\mathbf{F} - \frac{\partial\overline{u}}{\partial t}a\cos\varphi\right)_{\varphi=\text{const}} dp'\right], \tag{19}$$

where

$$\int_{p_1}^{p_2}\left(\nabla\cdot\mathbf{F} - \frac{\partial\overline{u}}{\partial t}a\cos\varphi\right)_{\varphi=\text{const}} dp \tag{20}$$

is referred to as the adjusted wave forcing.

Figure 12 shows the latitudinal distribution of the contemporary correlation coefficients between the PC 1 of the high-pass filtered and deseasonalized T^* at the 70-hPa level and the high-pass filtered and deseasonalized adjusted wave forcing expressed by (20). In comparison with Fig. 11a, Fig. 12a illustrates that wave forcing between 22.5° and 65° latitude coherently, significantly, and more negatively correlates with PC 1 at the 95% confidence level when 6-hourly ERA-40 data are used. In comparison with Fig. 11b, Fig. 12b shows that the wave forcing between 52.5° and 67.5° latitude is significantly and more negatively correlated with PC 1 at the 95% confidence level when monthly mean ERA-40 data are used. Thus, we conclude that subtropical wave forcing indeed plays an important role in driving the tropical upwelling portion of the Brewer–Dobson circulation on intraseasonal time scales, and that the effects of transient eddies are important and must be considered. By showing that higher correlations are obtained when the term is included in the right-hand side of (18) and comparing Figs. 11 and 12, we also illustrate the limitation of applying steady-state downward control.

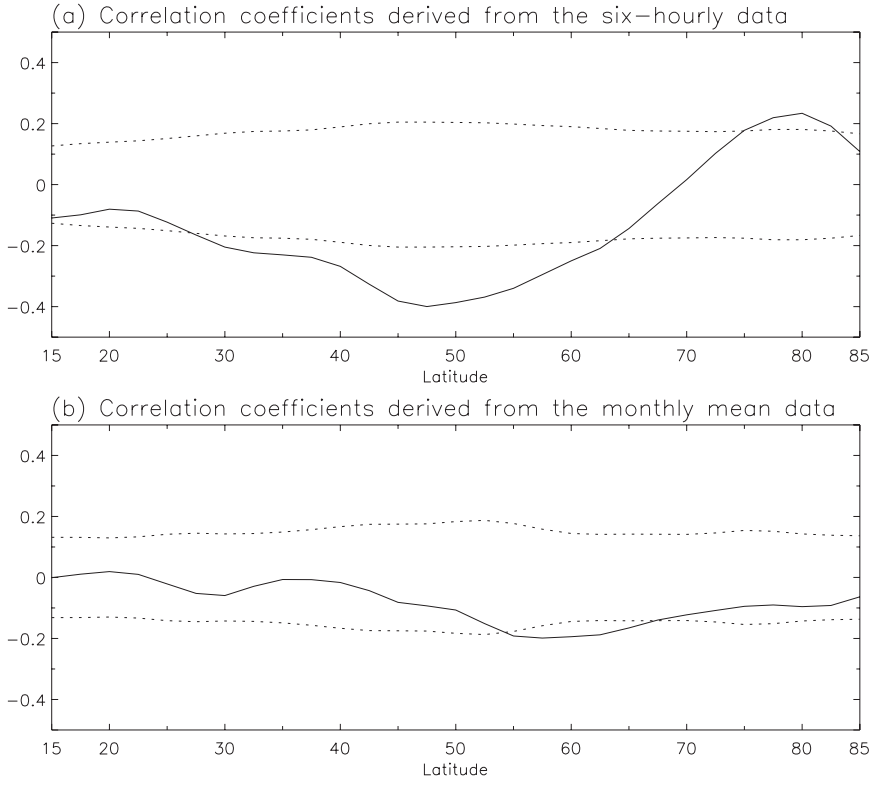

FIG. 11. As in Fig. 7, but for the high-pass filtered and deseasonalized T^* at the 70-hPa level and the corresponding wave forcing.

5. Discussion and conclusions

The recent paper by Ueyama and Wallace (2010) found that tropical upwelling into the lower stratosphere is mainly under the control of high-latitude wave driving. This is a surprising result in light of previous theoretical works (e.g., Plumb and Eluszkiewicz 1999; Semeniuk and Shepherd 2001; Zhou et al. 2006) that showed that the near-equatorial and subtropical wave driving were crucial in maintaining annually averaged tropical upwelling. This has motivated us to essentially redo the Ueyama and Wallace (2010) analysis using datasets with more frequent time sampling to see how this might alter their conclusions.

The main results of our analyses are as follows:

1) At the 70-hPa level, the temperature seesaw associated with variations of the BDC accounts for 90.1% of the month-to-month variance of the temporal variations about the annual-mean latitudinal distribution. This dynamic mode is dominated by the annual cycle (i.e., the equator-to-subpolar temperature contrast is largest in January/February and smallest in July/August.
2) The turnaround latitude associated with the annual cycle of the BDC shifts poleward with increasing height below 30 hPa in the lower stratosphere. At the 70-hPa level, it is approximately equal to 37.5°, which is comparable to the value derived from UKMO analysis and the results from various GCMs.
3) At the 70-hPa level, the temperature seesaw associated with nonseasonal variations of the BDC accounts for 57.5% of the month-to-month variance of the temporal variations about the climatological mean annual cycle of latitudinal temperature distribution. The turnaround latitude associated with nonseasonal variations of the BDC is the same as that associated with the annual cycle of the BDC. The nonseasonal variability of subtropical wave forcing is coherently and significantly correlated with that of the BDC in the lower stratosphere.
4) At the 70-hPa level, the temperature seesaw associated with interannual variations of the BDC accounts for 58.2% of the month-to-month variance of the temporal variations in the low-pass filtered and deseasonalized latitudinal temperature distribution. The turnaround latitude associated with interannual variations of the BDC is located near 22.5°. The interannual variability of subtropical wave forcing is indeed coherently and significantly correlated with that of the BDC in the lower stratosphere.

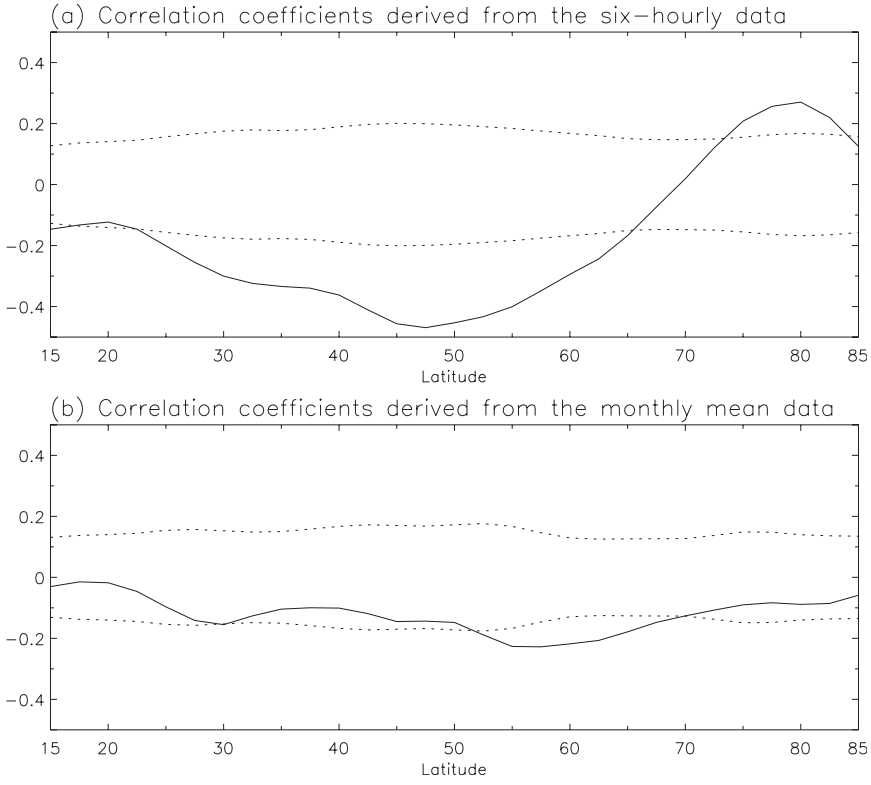

FIG. 12. As in Fig. 7, but for the high-pass filtered and deseasonalized T^* at the 70-hPa level and the corresponding adjusted wave forcing.

5) At the 70-hPa level, the temperature seesaw associated with interannual variations of the BDC exhibits a QBO variation. This is consistent with the fact that its interannual variability is significantly correlated with the vertical shear of the equatorial mean zonal wind at that level.
6) At the 70-hPa level, the temperature seesaw associated with intraseasonal variations of the BDC accounts for 76.0% of the month-to-month variance of the temporal variations in the high-pass filtered and deseasonalized latitudinal temperature distribution. The turnaround latitude associated with intraseasonal variations of the BDC is located near 47.5°. The intraseasonal variability of subtropical wave forcing is physically and significantly correlated with that of the BDC in the lower stratosphere.
7) Effects of transient eddies are important and must be considered. Very different conclusions are reached regarding latitudinal ranges over which the wave forcing (e.g., Eliassen–Palm flux convergence) contributes to the forcing of the tropical upwelling part of the Brewer–Dobson circulation when 6-hourly data are used instead of monthly mean and pentad data that were used by Ueyama and Wallace (2010) since these infrequent data samplings do not properly resolve transient wave forcing.
8) Subtropical wave forcing plays a crucial role in driving the tropical upwelling portion of the Brewer–Dobson circulation on various time scales when the effects of transient waves are properly considered.

We confirm Ueyama and Wallace's (2010) finding that wave forcing in the stratospheric ''surf zone'' plays an important role in driving tropical upwelling in the BDC on various time scales. However, since tropical upwelling in the BDC is coherently and significantly correlated with wave forcings in both the subtropical and the stratospheric surf zone regions, we conclude that wave forcings in those regions act synergistically to drive tropical upwelling in the BDC. Although wave forcing near the turnaround latitudes can largely control the strength of the BDC (Rosenlof 1995; Butchart and Scaife 2001; Fomichev et al. 2007; Shepherd and McLandress 2011), the latitudinal distribution of the residual mean vertical velocity, thus the turnaround latitude per se, is determined jointly by both low-latitude and higher-latitude wave forcings.

Butchart and Scaife (2001) showed that increased tropical upwelling in response to increased greenhouse

gas concentration–induced climate change results from strengthened wave forcing in the subtropical lower stratosphere, which in turn is largely caused by the increased penetration of resolved waves into that region due to the amplified zonal winds there. Fomichev et al. (2007) also showed that the enhanced tropical upwelling of the BDC is linked to increases in subtropical wave forcing rather than changes in wave forcing at higher latitudes.

Although climate models project the enhancement of tropical upwelling as a result of climate change (Butchart et al. 2006, 2010), consensus has not yet been reached on the exact manner in which tropical upwelling in the lower stratosphere is increased by wave forcing. Rind et al. (1990, 1998) argued that the increases in resolved wave forcing arise from increased generation of planetary waves due to decreases in large-scale static stability, and from improved propagation conditions associated with changes in refractive index due to strengthened upper flank of the subtropical jets. Rind et al. (1990) also pointed out that increased gravity wave forcing results from greater wave generation in response to climate changes, and from higher breaking altitudes of gravity waves due to strengthened upper flank of the subtropical jets, leading to more gravity wave momentum fluxes transferred into the stratosphere, which is confirmed by Li et al. (2008) and McLandress and Shepherd (2009). However, Butchart and Scaife (2001) and McLandress and Shepherd (2009) showed a strengthened BDC without any discernible change in refractive index.

Plumb (2002) depicted a paradigm where the BDC is driven by both planetary waves and synoptic waves. McLandress and Shepherd (2009) showed that together with parameterized orographic gravity wave forcing, both planetary waves and synoptic waves contribute to the enhancement of tropical upwelling. Shepherd and McLandress (2011) revealed that transient waves account for 80% of the contribution of resolved waves to the strengthened BDC in response to increased greenhouse gas concentration–induced climate change with roughly equal contributions from planetary waves and synoptic waves. Shepherd and McLandress (2011) further demonstrated that the strengthened upper flank of the subtropical jets leads to the uplifting of the critical layer associated with Rossby wave breaking (Randel and Held 1991), which in turn makes for more Rossby wave activity penetrating into the subtropical lower stratosphere, giving rise to strengthened transient wave forcing there. Thus, critical-layer control of wave breaking provides a unified theoretical framework within which gravity waves and transient waves of both planetary and synoptic scale give rise to enhanced subtropical wave forcing in the lower stratosphere in response to increased greenhouse gas concentration–induced climate change.

Although reanalysis data in the deep tropics are not reliable to evaluate the wave forcing there, we have found that the interannual variability of the BDC is significantly correlated with the vertical shear of the equatorial mean zonal wind. Wallace and Holton (1968) and Holton (1968) conclusively demonstrated that tropical wave forcing is required to account for the QBO of the zonal wind in the tropical stratosphere. Tropical wave forcing plays an indirect role in driving the tropical upwelling portion of the Brewer–Dobson circulation through its action on the zonal mean flow. Kerr-Munslow and Norton (2006) and Norton (2006) showed that tropical stationary waves drive the annual cycle in tropical tropopause temperatures while Garny et al. (2011) showed that tropical stationary waves play a leading role in the acceleration of upwelling velocities in the deep tropics in response to increases in greenhouse gases.

Thus, we conclude that both low-latitude and high-latitude wave forcing are important in driving tropical upwelling in the Brewer–Dobson circulation. In particular, the relative strengths of these forcings are important in determining the latitudinal distribution of the tropical upwelling, which in turn is crucial in determining the stratospheric ozone distribution.

Acknowledgments. This work was supported by NASA's Modeling and Analysis and Atmospheric Composition, Modeling and Analysis programs. We also acknowledge helpful suggestions from two anonymous reviewers.

REFERENCES

Andrews, D. G., J. D. Mahlman, and R. W. Sinclair, 1983: Eliassen–Palm diagnostics of wave–mean flow interaction in the GFDL "SKYHI" general circulation model. *J. Atmos. Sci.,* **40,** 2768–2784.

——, J. R. Holton, and C. B. Leovy, 1987: *Middle Atmosphere Dynamics*. Academic Press, 489 pp.

Austin, J., and F. Li, 2006: On the relationship between the strength of the Brewer–Dobson circulation and the age of stratospheric air. *Geophys. Res. Lett.,* **33,** L17807, doi:10.1029/2006GL026867.

——, J. Wilson, F. Li, and H. Vömel, 2007: Evolution of water vapor concentrations and stratospheric age of air in coupled chemistry–climate model simulations. *J. Atmos. Sci.,* **64,** 905–921.

Baldwin, M. P., and Coauthors, 2001: The quasi-biennial oscillation. *Rev. Geophys.,* **39,** 179–229.

Bergman, J. W., and M. L. Salby, 1994: Equatorial wave activity derived from fluctuations in observed convection. *J. Atmos. Sci.,* **51,** 3791–3806.

Boehm, M. T., and S. Lee, 2003: The implications of tropical Rossby waves for tropical tropopause cirrus formation and for the equatorial upwelling of the Brewer–Dobson circulation. *J. Atmos. Sci.,* **60,** 247–261.

Boering, K. A., S. C. Wofsy, B. C. Daube, H. R. Schneider, M. Loewenstein, J. R. Podoiske, and T. J. Conway, 1996: Stratospheric mean ages and transport rates from observations of carbon dioxide and nitrous oxide. *Science,* **274,** 1340–1343.

Brewer, A. W., 1949: Evidence for a world circulation provided by the measurements of helium and water vapour distribution in the stratosphere. *Quart. J. Roy. Meteor. Soc.,* **75,** 351–363.

Butchart, N., and A. A. Scaife, 2001: Removal of chlorofluorocarbons by increased mass exchange between the stratosphere and the troposphere in a changing climate. *Nature,* **410,** 799–802.

——, J. Austin, K. R. Knight, A. A. Scaife, and K. L. Gallani, 2000: The response of the stratospheric climate to projected changes in the concentrations of well-mixed greenhouse gases from 1992 to 2051. *J. Climate,* **13,** 2142–2159.

——, and Coauthors, 2006: Simulations of anthropogenic change in the strength of the Brewer–Dobson circulation. *Climate Dyn.,* **27,** 727–741, doi:10.1007/s00382-006-0162-4.

——, and Coauthors, 2010: Chemistry–climate model simulations of twenty-first century stratospheric climate and circulation changes. *J. Climate,* **23,** 5349–5374.

——, and Coauthors, 2011: Multimodel climate and variability of the stratosphere. *J. Geophys. Res.,* **116,** D05102, doi:10.1029/2010JD014995.

Chen, G., and L. Sun, 2011: Mechanisms of the tropical upwelling branch of the Brewer–Dobson circulation: The role of extratropical waves. *J. Atmos. Sci.,* **68,** 2878–2892.

Chun, H.-Y., Y.-H. Kim, H.-J. Choi, and J.-Y. Kim, 2011: Influence of gravity waves in the tropical upwelling: WACCM simulations. *J. Atmos. Sci.,* **68,** 2599–2612.

Dee, D. P., and Coauthors, 2011: The ERA-Interim reanalysis: Configuration and performance of the data assimilation system. *Quart. J. Roy. Meteor. Soc.,* **137,** 553–597.

Dobson, G. M. B., 1956: Origin and distribution of the polyatomic molecules in the atmosphere. *Proc. Roy. Soc. London,* **236A,** 187–193.

Dunkerton, T. J., 1978: On the mean meridional mass motions of the stratosphere and mesosphere. *J. Atmos. Sci.,* **35,** 2325–2333.

——, and M. P. Baldwin, 1991: Quasi-biennial modulation of planetary-wave fluxes in the Northern Hemisphere winter. *J. Atmos. Sci.,* **48,** 1043–1061.

Eichelberger, S. J., and D. L. Hartmann, 2005: Changes in the strength of the Brewer–Dobson circulation in a simple AGCM. *Geophys. Res. Lett.,* **32,** L15807, doi:10.1029/2005GL022924.

Fomichev, V. I., A. I. Jonsson, J. de Grandpré, S. R. Beagley, C. McLandress, K. Semeniuk, and T. G. Shepherd, 2007: Response of the middle atmosphere to CO_2 doubling: Results from the Canadian Middle Atmosphere Model. *J. Climate,* **20,** 1121–1144.

Fueglistaler, S., P. H. Haynes, and P. M. Forster, 2011: The annual cycle in lower stratospheric temperatures revisited. *Atmos. Chem. Phys.,* **11,** 3701–3711, doi:10.5194/acp-11-3701-2011.

Garcia, R. R., and W. J. Randel, 2008: Acceleration of the Brewer–Dobson circulation due to increases in greenhouse gases. *J. Atmos. Sci.,* **65,** 2731–2739.

——, ——, and D. E. Kinnison, 2011: On the determination of age of air trends from atmospheric trace species. *J. Atmos. Sci.,* **68,** 139–154.

Garny, H., M. Dameris, W. J. Randel, G. E. Bodeker, and R. Deckert, 2011: Dynamically forced increase of tropical upwelling in the lower stratosphere. *J. Atmos. Sci.,* **68,** 1214–1233.

Geller, M. A., T. Zhou, and K. Hamilton, 2008: Morphology of tropical upwelling in the lower stratosphere. *J. Atmos. Sci.,* **65,** 2360–2374.

Gill, A. E., 1982: *Atmosphere–Ocean Dynamics*. International Geophysics Series, Vol. 30, Academic Press, 662 pp.

Gille, J. C., L. V. Lyjak, and A. K. Smith, 1987: The global residual mean circulation in the middle atmosphere for the northern winter period. *J. Atmos. Sci.,* **44,** 1437–1452.

Giorgetta, M. A., E. Manzini, and E. Roeckner, 2002: Forcing of the quasi-biennial oscillation from a broad spectrum of atmospheric waves. *Geophys. Res. Lett.,* **29,** 1245, doi:10.1029/2002GL014756.

Gray, L. J., S. Crooks, C. Pascoe, S. Sparrow, and M. Palmer, 2004: Solar and QBO influences on the timing of stratospheric sudden warmings. *J. Atmos. Sci.,* **61,** 2777–2796.

Hall, T. M., and R. A. Plumb, 1994: Age as a diagnostic of stratospheric transport. *J. Geophys. Res.,* **99,** 1059–1070.

Haynes, P. H., 2005: Stratospheric dynamics. *Annu. Rev. Fluid Mech.,* **37,** 263–293.

——, and M. E. McIntyre, 1987: On the evolution of vorticity and potential vorticity in the presence of diabatic heating and frictional or other forces. *J. Atmos. Sci.,* **44,** 828–841.

——, C. J. Marks, M. E. McIntyre, T. G. Shepherd, and K. P. Shine, 1991: On the ''downward control'' of extratropical diabatic circulations by eddy-induced mean zonal forces. *J. Atmos. Sci.,* **48,** 651–678.

Holton, J. R., 1968: A note on the propagation of the biennial oscillation. *J. Atmos. Sci.,* **25,** 519–521.

——, 1990: On the global exchange of mass between the stratosphere and the troposphere. *J. Atmos. Sci.,* **47,** 392–395.

——, 2004: *An Introduction to Dynamical Meteorology*. 4th ed. Elsevier Academic, 535 pp.

——, and C. Mass, 1976: Stratospheric vacillation cycles. *J. Atmos. Sci.,* **33,** 2218–2225.

——, and H.-C. Tan, 1980: The influence of the equatorial quasi-biennial oscillation on the global circulation at 50 mb. *J. Atmos. Sci.,* **37,** 2200–2208.

——, and ——, 1982: The quasi-biennial oscillation in the Northern Hemisphere lower stratosphere. *J. Meteor. Soc. Japan,* **60,** 140–147.

——, P. H. Haynes, M. E. McIntyre, A. R. Douglass, R. B. Rood, and L. Pfister, 1995: Stratosphere–troposphere exchange. *Rev. Geophys.,* **33,** 403–439.

Kalnay, E., and Coauthors, 1996: The NCEP/NCAR 40-Year Reanalysis Project. *Bull. Amer. Meteor. Soc.,* **77,** 437–471.

Kerr-Munslow, A. M., and W. A. Norton, 2006: Tropical wave driving of the annual cycle in tropical tropopause temperatures. Part I: ECMWF analyses. *J. Atmos. Sci.,* **63,** 1410–1419.

Ko, M. K. W., K. K. Tung, D. K. Weisenstein, and N. D. Sze, 1985: A zonal-mean model of stratospheric tracer transport in isentropic coordinates: Numerical simulations for nitrous oxide nitric acid. *J. Geophys. Res.,* **90,** 2313–2329.

Labitzke, K., 1982: On the interannual variability of the middle stratosphere during the northern winters. *J. Meteor. Soc. Japan,* **60,** 124–139.

Li, F., J. Austin, and J. Wilson, 2008: The strength of the Brewer–Dobson circulation in a changing climate: Coupled chemistry–climate model simulations. *J. Climate,* **21,** 40–57.

McIntyre, M. E., 1990: Middle atmosphere dynamics and transport: Some current challenges to our understanding. *Dynamics, Transport and Photochemistry in the Middle Atmosphere of the Southern Hemisphere,* A. O'Neill, Ed., Kluwer, 1–18.

——, 1999: How far have we come in understanding the dynamics of the middle atmosphere? *Proceedings of the 14th European Space Symposium on European Rocket and Balloon Programmes and Related Research*, ESA SP-437, B. Kaldeich-Schürmann, Ed., ESA Publications, 581–590.

——, and T. N. Palmer, 1983: Breaking planetary waves in the stratosphere. *Nature,* **305,** 593–600.

——, and ——, 1984: The ''surf zone'' in the stratosphere. *J. Atmos. Terr. Phys.,* **46,** 825–849.

McLandress, C., and T. G. Shepherd, 2009: Simulated anthropogenic changes in the Brewer–Dobson circulation, including its extension to high latitudes. *J. Climate,* **22,** 1516–1540.

Mears, C., and F. J. Wentz, 2009: Construction of the Remote Sensing Systems v3.2 atmospheric temperature records from the MSU and AMSU microwave sounders. *J. Atmos. Oceanic Technol.,* **26,** 1040–1056.

Mote, P. W., and Coauthors, 1996: An atmospheric tape recorder: The imprint of tropical tropopause temperatures on stratospheric water vapor. *J. Geophys. Res.,* **101,** 3989–4006.

Murgatroyd, R. J., and F. Singleton, 1961: Possible meridional circulations in the stratosphere and mesosphere. *Quart. J. Roy. Meteor. Soc.,* **87,** 125–135.

Naoe, H., and K. Shibata, 2010: Equatorial quasi-biennial oscillation influence on northern winter extratropical circulation. *J. Geophys. Res.,* **115,** D19102, doi:10.1029/2009JD012952.

Niwano, M., K. Yamazaki, and M. Shiotani, 2003: Seasonal and QBO variations of ascent rate in the tropical lower stratosphere as inferred from UARS HALOE trace gas data. *J. Geophys. Res.,* **108,** 4794, doi:10.1029/2003JD003871.

North, G. R., T. L. Bell, R. F. Cahalan, and F. J. Moeng, 1982: Sampling errors in the estimation of empirical orthogonal functions. *Mon. Wea. Rev.,* **110,** 699–706.

Norton, W. A., 2006: Tropical wave driving of the annual cycle in tropical tropopause temperatures. Part II: Model results. *J. Atmos. Sci.,* **63,** 1420–1431.

Oman, L., D. W. Waugh, S. Pawson, R. S. Stolarski, and P. A. Newman, 2009: On the influence of anthropogenic forcings on changes in the stratospheric mean age. *J. Geophys. Res.,* **114,** D03105, doi:10.1029/2008JD010378.

Oort, A. H., and J. J. Yienger, 1996: Observed interannual variability in the Hadley circulation and its connection to ENSO. *J. Climate,* **9,** 2751–2767.

Plumb, R. A., 2002: Stratospheric transport. *J. Meteor. Soc. Japan,* **80,** 793–809.

——, and R. C. Bell, 1982: A model of the quasi-biennial oscillation on an equatorial beta-plane. *Quart. J. Roy. Meteor. Soc.,* **108,** 335–352.

——, and J. Eluszkiewicz, 1999: The Brewer–Dobson circulation: Dynamics of the tropical upwelling. *J. Atmos. Sci.,* **56,** 868–890.

Powell, A., and J. Xu, 2010: Uncertainties of the relationship between the equatorial quasi-biennial oscillation, the Arctic stratosphere and solar forcing. *J. Atmos. Terr. Phys.,* **72,** 1354–1363.

Randel, W. J., and I. M. Held, 1991: Phase speed spectra of transient eddy fluxes and critical layer absorption. *J. Atmos. Sci.,* **48,** 688–697.

——, F. Wu, J. M. Russell III, and J. Waters, 1999a: Space-time patterns of trends in stratospheric constituents derived from UARS measurements. *J. Geophys. Res.,* **104,** 3711–3727.

——, ——, R. Swinbank, J. Nash, and A. O'Neill, 1999b: Global QBO circulation derived from UKMO stratospheric analyses. *J. Atmos. Sci.,* **56,** 457–474.

——, R. R. Garcia, and F. Wu, 2002: Time-dependent upwelling in the tropical lower stratosphere estimated from the zonal-mean momentum budget. *J. Atmos. Sci.,* **59,** 2141–2152.

——, and Coauthors, 2004: The SPARC intercomparison of middle-atmosphere climatologies. *J. Climate,* **17,** 986–1003.

——, F. Wu, H. Vömel, G. E. Nedoluha, and P. Forster, 2006: Decreases in stratospheric water vapor since 2001: Links to changes in the tropical tropopause and the Brewer–Dobson circulation. *J. Geophys. Res.,* **111,** D12312, doi:10.1029/2005JD006744.

——, R. R. Garcia, and F. Wu, 2008: Dynamical balances and tropical stratospheric upwelling. *J. Atmos. Sci.,* **65,** 3584–3595.

Reed, R. J., 1964: A tentative model of the 26-month oscillation in tropical latitudes. *Quart. J. Roy. Meteor. Soc.,* **90,** 441–466.

——, and C. L. Vlcek, 1969: The annual temperature variation in the lower tropical stratosphere. *J. Atmos. Sci.,* **26,** 163–167.

Rind, D., R. Suozzo, N. K. Balachandran, and M. J. Prather, 1990: Climate change and the middle atmosphere. Part I: The doubled CO_2 climate. *J. Atmos. Sci.,* **47,** 475–494.

——, D. Shindell, P. Lonergan, and N. K. Balachandran, 1998: Climate change and the middle atmosphere. Part III: The doubled CO_2 climate revisited. *J. Climate,* **11,** 876–894.

Rosenfield, J. E., M. R. Schoeberl, and M. A. Geller, 1987: A computation of the stratospheric diabatic circulation using an accurate radiative transfer model. *J. Atmos. Sci.,* **44,** 859–876.

Rosenlof, K. H., 1995: Seasonal cycle of the residual mean meridional circulation in the stratosphere. *J. Geophys. Res.,* **100,** 5173–5191.

——, and J. R. Holton, 1993: Estimates of the stratospheric residual circulation using the downward control principle. *J. Geophys. Res.,* **98,** 10 465–10 479.

Ruzmaikin, A., J. Feynman, X. Jiang, and Y. L. Yung, 2005: Extratropical signature of the quasi-biennial oscillation. *J. Geophys. Res.,* **110,** D11111, doi:10.1029/2004JD005382.

Ryu, J.-H., and S. Lee, 2010: Effect of tropical waves on the tropical tropopause transition layer upwelling. *J. Atmos. Sci.,* **67,** 3130–3148.

Salby, M. L., 2011: Interannual changes of stratospheric temperature and ozone: Forcing by anomalous wave driving and the QBO. *J. Atmos. Sci.,* **68,** 1513–1525.

——, and P. F. Callaghan, 2002: Interannual changes of the stratospheric circulation: Relationship to ozone and tropospheric structure. *J. Climate,* **15,** 3673–3685.

Scott, R. K., 2002: Wave-driven mean tropical upwelling in the lower stratosphere. *J. Atmos. Sci.,* **59,** 2745–2759.

Semeniuk, K., and T. G. Shepherd, 2001: Mechanisms for tropical upwelling in the stratosphere. *J. Atmos. Sci.,* **58,** 3097–3115.

Shepherd, T. G., and C. McLandress, 2011: A robust mechanism for strengthening of the Brewer–Dobson circulation in response to climate change: Critical-layer control of subtropical wave breaking. *J. Atmos. Sci.,* **68,** 784–797.

Shine, K., 1989: Sources and sinks of zonal momentum in the middle atmosphere diagnosed using the diabatic circulation. *Quart. J. Roy. Meteor. Soc.,* **115,** 265–292.

Sigmond, M., P. C. Siegmund, E. Manzini, and H. Kelder, 2004: A simulation of the separate climate effects of middle-atmospheric and tropospheric CO_2 doubling. *J. Climate,* **17,** 2352–2367.

Simpson, I. R., T. G. Shepherd, and M. Sigmond, 2011: Dynamics of the lower stratospheric circulation response to ENSO. *J. Atmos. Sci.,* **68,** 2537–2556.

Solomon, S., J. T. Kiehl, R. R. Garcia, and W. Grose, 1986: Tracer transport by the diabatic circulation deduced from satellite observations. *J. Atmos. Sci.,* **43,** 1603–1617.

Spiegel, M. R., J. J. Schiller, and R. A. Srinivasan, 2008: *Schaum's Outlines Probability and Statistics*. 3rd ed. McGraw-Hill, 432 pp.

Thompson, D. W. J., and J. M. Wallace, 2000: Annular modes in the extratropical circulation. Part I: Month-to-month variability. *J. Climate,* **13,** 1000–1016.

Ueyama, R., and J. M. Wallace, 2010: To what extent does high-latitude wave forcing drive tropical upwelling in the Brewer–Dobson circulation? *J. Atmos. Sci.,* **67,** 1232–1246.

Uppala, S. M., and Coauthors, 2005: The ERA-40 Re-Analysis. *Quart. J. Roy. Meteor. Soc.,* **131,** 2961–3012.

Wallace, J. M., and J. R. Holton, 1968: A diagnostic numerical model of the quasi-biennial oscillation. *J. Atmos. Sci.,* **25,** 280–292.

——, and F.-C. Chang, 1982: Interannual variability of the wintertime polar vortex in the Northern Hemisphere middle stratosphere. *J. Meteor. Soc. Japan,* **60,** 149–155.

Watanabe, S., Y. Kawatani, Y. Tomikawa, K. Miyazaki, M. Takahashi, and K. Sato, 2008: General aspects of a T213L256 middle atmosphere general circulation model. *J. Geophys. Res.,* **113,** D12110, doi:10.1029/2008JD010026.

Waugh, D. W., 1996: Seasonal variation of isentropic transport out of the tropical stratosphere. *J. Geophys. Res.,* **101,** 4007–4023.

——, 2009: The age of stratospheric air. *Nat. Geosci.,* **2,** 14–16.

——, and T. Hall, 2002: Age of stratospheric air: Theory, observations, and models. *Rev. Geophys.,* **40,** 1010, doi:10.1029/2000RG000101.

WMO/UNEP, 2011: Scientific assessment of ozone depletion: 2010. Global Ozone Research and Monitoring Project Rep. 52. [Available online at http://ozone.unep.org/Assessment_Panels/SAP/Scientific_Assessment_2010/index.shtml.]

Yoden, S., 1987: Bifurcation properties of a stratospheric vacillation. *J. Atmos. Sci.,* **44,** 1723–1733.

Yulaeva, E., J. R. Holton, and J. M. Wallace, 1994: On the cause of the annual cycle in tropical lower-stratospheric temperatures. *J. Atmos. Sci.,* **51,** 169–174.

Zhou, T., M. A. Geller, and K. Hamilton, 2006: The roles of the Hadley circulation and downward control in tropical upwelling. *J. Atmos. Sci.,* **63,** 2740–2757.

Zhou, X.-L., M. A. Geller, and M. Zhang, 2001: Cooling trend of the tropical cold point tropopause temperatures and its implications. *J. Geophys. Res.,* **106,** 1511–1521.